

Numerical investigation and recurrence plot analysis of pulsating magnetohydrodynamic mixed convection over a backward facing step

Fatih Selimefendigil

Department of Mechanical Engineering
Celal Bayar University
Manisa, Turkey
fatih.selimefendigil@cbu.edu.tr

Received: June 17, 2013 / **Revised:** October 21, 2014 / **Published online:** March 31, 2015

Abstract. In the current study, numerical investigation of pulsating magnetohydrodynamic mixed convection over a backward facing step is carried out for the range of parameters; Reynolds number ($25 \leq Re \leq 100$), Hartmann number ($0 \leq Ha \leq 60$), Strouhal number ($0.1 \leq St \leq 1$) and Gr number is kept at $Gr = 10^4$. The governing equations are solved with a general purpose finite element based solver. The effects of various parameters on the fluid flow and heat transfer characteristics are numerically studied. It is observed that the flow field and heat transfer rate are influenced by the variations of Reynolds, Hartmann and Strouhal numbers. Furthermore, recurrence plot analysis is applied for the analysis of the time series (spatial averaged Nusselt number along the bottom wall downstream of the step) and for a combination of different parameters, the systems are identified using recurrence quantification analysis parameters including recurrence rate, laminarity, determinism, trapping time and entropy.

Keywords: backward facing step, MHD flow, recurrence quantification analysis, nonlinear time series.

1 Introduction

The flow over a backward facing or forward facing step is an important problem in many engineering applications such as flow around airfoils, buildings, combustors and collectors of power systems. A comprehensive review is presented in [1] for laminar mixed convection over vertical, horizontal and inclined backward- and forward-facing steps studied in the open literature. In this review, the effects of pertinent parameters such as Reynolds number, Prandtl number and expansion ratio on the fluid flow and thermal characteristics is also presented.

A vast amount of literature is dedicated to that subject either numerically [6, 7, 16, 30, 32, 33] or experimentally [2, 4, 37, 39]. 3D linear stability analysis of flow over a backward-facing step for Reynolds numbers between 450 and 1050 was studied in [7]. Velocity

distribution and reattachment length using Laser-Doppler measurement for flow downstream of a backward facing step in a two-dimensional channel was reported in [4]. Their results showed separation length varies with Reynolds number and various flow regimes are characterized by variations of the separation length.

Mixed convection magnetohydrodynamics flows of electrically conducting fluid has many industrial applications such as coolers of nuclear reactors, micro-electronic devices, purification of molten metals many others. Due to the effect of the magnetic field, the fluid flow experiences a Lorentz force. Employing an external magnetic field can be used as a control method since magnetic field can suppress the convective flow field Rahman10, [34, 35, 36]. Mixed convection with a magnetic field in a top sided lid-driven cavity heated by a corner heater was studied in ref. [27]. They showed that heat transfer decreases with increasing the Hartmann number and magnetic field plays an important role to control heat transfer and fluid flow. Steady laminar magnetohydrodynamic mixed convection heat transfer about a vertical slender cylinder was analyzed in [5]. A uniform magnetic field was applied perpendicular to the cylinder. They observed that the local skin friction coefficient and the local heat transfer coefficient increase, increasing the Richardson number, electric field parameter and magnetic parameter. Steady, laminar natural convection in the presence of a magnetic field in a tilted enclosure heated from below was numerically studied in [28]. Their results showed that for a given inclination angle, as the value of Hartmann number increases, the convection heat transfer reduces. Steady magnetohydrodynamic mixed convection flow adjacent to a vertical surface with prescribed heat flux was investigated in [19]. They found that magnetic parameter plays an important role in controlling the boundary layer separation.

In the present study, numerical investigation of pulsating magnetohydrodynamic mixed convection over a backward facing step is carried out for a range of Reynolds number, Hartmann number and Strouhal number. The effects of these parameters on the flow and heat transfer are investigated. Furthermore, time series data obtained from spatial averaged Nusselt number along the bottom wall of the cavity downstream of the step is analyzed using recurrence plots. Recurrence quantification analysis parameters including recurrence rate, laminarity, determinism, trapping time and entropy are also provided to quantify the nonlinear time series of Nusselt numbers for different combinations of Reynolds, Hartmann and Strouhal numbers.

2 Numerical simulation

2.1 Problem description

A schematic description of the physical problem considered in this study is shown in Fig. 1. A channel with a backward facing step is considered. The step size of backward facing step is H and channel height is $2H$. Total length of the channel is 1 m. At the inlet of the channel, a parabolic velocity with a sinusoidal time dependent part ($u = u_0 + 0.75u_0 \sin(2\pi ft)$) and a uniform temperature ($T = 300$ K) is imposed. It was confirmed from numerical simulation that, the flow is developed before reaching the step. The downstream length starting from the edge of the step to the exit of the channel is

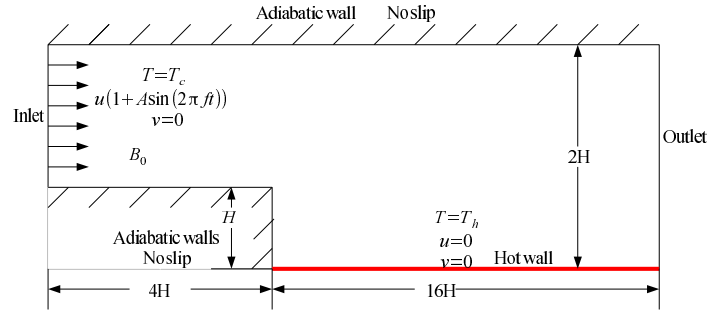


Fig. 1. Geometry with boundary conditions.

$16H$ to ensure that the recirculation length downstream of the step is independent of the computational domain. The downstream bottom surface of the backward facing step is maintained at $T = 310$ K, while the other walls of the channel are assumed to be adiabatic. Working fluid is air with a Prandtl number of $Pr = 0.71$. It is assumed that thermo-physical properties of the fluid is temperature independent. Fluid properties are taken at the average temperature of 305 K. The variations of the physical properties with temperature are neglected. Only 2.5% of maximum deviation is observed with constant property assumption.

The flow is assumed to be two dimensional, Newtonian, incompressible and in the laminar flow regime. The three dimensional effects of the flow over a backward facing step have been studied in references [9,41]. [29] have studied the MHD mixed convection in an open channel with a square cavity which has a partially or fully heated on left side using finite element method. The range of parameters studied by [29] was: $10^4 \leq Ra \leq 10^6$; $0 \leq Ha \leq 100$ and $Re = 100$. In our study, $Gr = 10^4$, $Re = 100$ and $0 \leq Ha \leq 60$. Therefore, our model problem is also treated as two dimensional. The three dimensional effects and the possible effect of the presence of side walls on flow field and heat transfer are out of the scope of the present paper. [12] and [18] have studied the transition in wall bounded unsteady flow. They proposed to use Reynolds number based on Stokes layer thickness which is given as

$$\delta = \left(\frac{2\nu}{\omega} \right)^{1/2}, \quad (1)$$

where ν and ω denote kinematic viscosity of the fluid and dimensional pulsation frequency, respectively. The smallest value of Strouhal number is 0.1 and based on this $Re_\delta = 300$ which is less than the critical value for the transition. Therefore, laminar behavior of the flow is justified.

A uniform magnetic field with strength B_0 is applied in the direction of the velocity. The field induced by the fluid motion is considered to be negligible compared to the applied field. A term is added in the momentum equation which corresponds to the Lorentz force induced by the interaction of the magnetic field with the convective motion. Hall effect of magnetohydrodynamics is assumed to be negligible and magnetic Reynolds number is assumed to be small [29].

By using the dimensionless parameters

$$(U, V) = \frac{(u, v)}{u_0}, \quad (X, Y) = \frac{(x, y)}{H}, \quad P = \frac{\bar{p}}{\rho u_0^2}, \quad \theta = \frac{T - T_c}{T_h - T_c} \quad (2)$$

for a two dimensional, incompressible, laminar and unsteady case, the continuity, momentum and energy equations can be expressed in the nondimensional form as in the following [29]:

$$\frac{\partial U}{\partial X} + \frac{\partial V}{\partial Y} = 0, \quad (3)$$

$$\frac{\partial U}{\partial \tau} + U \frac{\partial U}{\partial X} + V \frac{\partial U}{\partial Y} = -\frac{\partial P}{\partial X} + \frac{1}{Re} \left(\frac{\partial^2 U}{\partial X^2} + \frac{\partial^2 U}{\partial Y^2} \right), \quad (4)$$

$$\frac{\partial V}{\partial \tau} + U \frac{\partial V}{\partial X} + V \frac{\partial V}{\partial Y} = -\frac{\partial P}{\partial Y} + \frac{1}{Re} \left(\frac{\partial^2 V}{\partial X^2} + \frac{\partial^2 V}{\partial Y^2} \right) + \frac{Gr}{Re^2} \Theta - \frac{Ha^2}{Re} V, \quad (5)$$

$$\frac{\partial \theta}{\partial \tau} + U \frac{\partial \theta}{\partial X} + V \frac{\partial \theta}{\partial Y} = \frac{1}{Re Pr} \left(\frac{\partial^2 \theta}{\partial X^2} + \frac{\partial^2 \theta}{\partial Y^2} \right). \quad (6)$$

The relevant physical nondimensional numbers are Reynolds number (Re), Grashof number (Gr), Hartmann number (Ha) and Strouhal number (St):

$$Re = \frac{u_0 H}{\nu}, \quad Gr = \frac{g \beta (T_h - T_c) H^3}{\nu^2}, \quad Ha = B_0 H \sqrt{\frac{\sigma}{\rho \mu}}, \quad St = \frac{f H}{u_0}. \quad (7)$$

The boundary conditions for the considered problem in dimensional form can be expressed as:

- At the inlet, velocity is unidirectional sinusoidal, temperature and velocity are uniform ($u = u_0(1 + A \sin(2\pi ft))$, $v = 0$, $T = T_c$).
- At the bottom wall, downstream of the step, temperature is constant ($T = T_h$).
- At the channel exit, outlet boundary condition (pressure, no viscous stress), ($\mu(\nabla \mathbf{u} + (\nabla \mathbf{u})^T) \mathbf{n} = \mathbf{0}$, $p = p_0$) and convective flux ($\mathbf{n}(-k \nabla T)$) boundary condition were used.
- On the channel walls (except the downstream of the step), adiabatic wall with no-slip boundary conditions are assumed, ($u = 0$, $v = 0$, $\partial T / \partial n = 0$).

Local Nusselt number is defined as

$$Nu_{x,t} = \frac{h_{x,t} L}{k} = - \left(\frac{\partial \theta}{\partial n} \right)_S, \quad (8)$$

where $h_{x,t}$ represent the local heat transfer coefficient and k denote the thermal conductivity of air. Spatial averaged Nusselt number is obtained after integrating the local Nusselt number along the bottom wall downstream of the step as

$$Nu_t = \frac{1}{L} \int_0^L Nu_{x,t} dx. \quad (9)$$

Time and spatial averaged Nusselt number is obtained after integrating spatial averaged Nusselt number along the bottom wall downstream of the step for one period of the oscillation τ as

$$Nu_m = \frac{1}{\tau} \int_0^{\tau} Nu_t dt. \quad (10)$$

Equations (3)–(6) along with the boundary conditions are solved with COMSOL Multiphysics (a general purpose finite element solver [11]). Lagrange finite elements of different orders are used to discretize velocity components, pressure and temperature. The finite element formulation is obtained by establishing the weak form the governing equations with Galerkin procedure. The computational domain is divided into non-overlapping regions within each of the flow variables are approximated by using the interpolation functions. In order to avoid the need for stabilizing convective terms in momentum equations, meshes are resolved fine enough. COMSOL solver adds artificial diffusion with the streamline upwind Petrov–Galerkin method (SUPG) to handle local numerical instabilities. Segregated parametric solvers are used for fluid flow and heat transfer variables. Biconjugate gradient stabilized iterative method solver (BICGSTab) is used for fluid flow and heat transfer modules of this software.

The unstructured body-adapted mesh of appropriate size consists of only triangular elements. In order to avoid the need for stabilizing convective terms in momentum equations, meshes are resolved fine enough. The computational domain is divided into 30799 triangular elements. The mesh is finer near the walls to resolve the high gradients in the thermal and hydrodynamic boundary layer and in the vicinity of the step for the recirculation region downstream of the step. Mesh independence study is also carried out to obtain an optimal grid distribution with accurate results and minimal computational time. Five different grid sizes are tested and the convergence in the length-averaged Nusselt number (along the bottom wall downstream of the step) is checked. The results at Reynolds number of 100, $Ha = 60$ are tabulated in Table 1. From this table, grid size of 30799 is decided to be fine enough to resolve the flow and thermal field.

The numerical code is first checked against the benchmarked results of backward facing step reported in the literature [3, 10, 13, 15, 22]. Table 2 shows the results of the reattachment length divided by step height at Reynolds number of 100 for expansion ratio of 2. Minimum deviation for the percentage in the error is obtained for the results of [3] which is -0.2 percent. The agreement between the other sources is less than 5 percent, only -6.8 percent error is obtained for the results of [10]. The present code is further validated with the results computed in [21]. Local Nusselt number along the bottom wall downstream of the step is shown in Fig. 2 for various Reynolds numbers and the overall trend is similar.

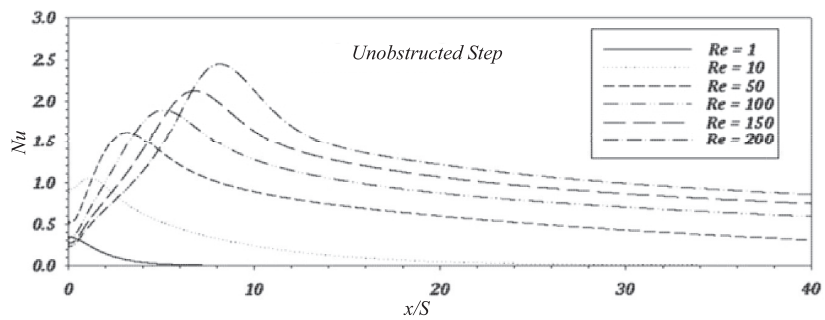
Steady simulation results are used as the initial condition for the unsteady computations. Time step size independence study is carried out. Considering both accuracy and computational time of the simulation a time step size of $(1/100)$ th of the period of the pulsating flow is chosen in this study.

Table 1. Length averaged Nusselt numbers on the bottom wall downstream of the step for different grid densities.

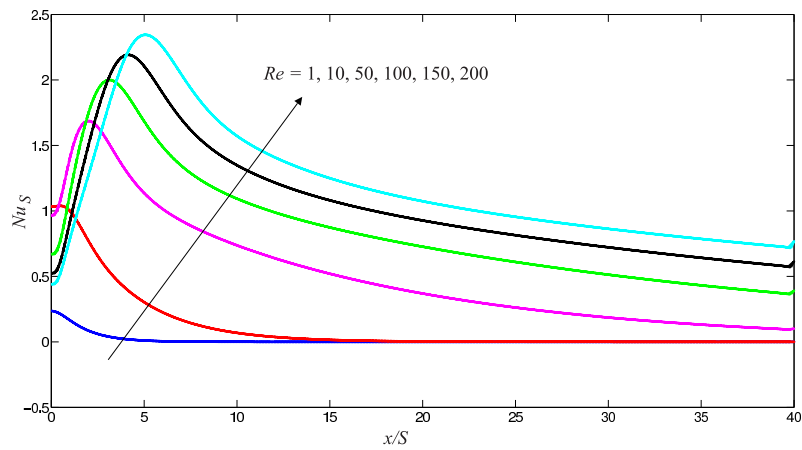
| Grid size | Averaged Nusselt number | Grid size | Averaged Nusselt number |
|-----------|-------------------------|--------------|-------------------------|
| 3463 | 0.6203 | 30779 | 0.6084 |
| 7456 | 0.6108 | 62288 | 0.6084 |
| 15170 | 0.6081 | | |

Table 2. Reported values for the reattachment lengths X_R at Reynolds number 100 (expansion ratio of 2).

| | X_R/S | Error (%) |
|-----------------------|---------|-----------|
| Present | 4.98 | 0 |
| Acharya et al. [3] | 4.97 | -0.2 |
| Lin et al. [22] | 4.91 | -1.4 |
| Dyne et al. [13] | 4.89 | -1.8 |
| El-Refaee et al. [15] | 4.77 | -4.21 |
| Cochran et al. [10] | 5.32 | 6.82 |



(a) ref. [21]



(b) present code

Fig. 2. Comparison of local Nusselt numbers computed in [21] and computed with the present code.

3 Nonlinear time series analysis

The nonlinear time series analysis methods can be used to study and gain an understanding of the complicated nonlinear dynamical system. The time sequence of the acoustic velocity at the heater location (u_0, \dots, u_n) is obtained from the numerical simulation. According to [38], the reconstructed attractor of the original system is given by

$$U(i) = (u_i, u_{i+\tau}, \dots, u_{i+(m-1)\tau}) \quad (11)$$

with τ and m representing the embedding delay and embedding dimension, respectively. The attractor constructed using the above equation will have the same mathematical features of the original system, such as dimension, Lyapunov exponents, etc. The delayed variable $u_{i+\tau}$ carries information about the influences of all other variables during time τ . One can introduce the third $u_{i+2\tau}$ and m th $u_{i+(m-1)\tau}$ variable and obtain the whole m -dimensional phase space where the variables incorporate all the influences of the original system provided that m is large enough.

To get an estimate for delay term τ autocorrelation function or average mutual information function can be used. The latter takes into account the nonlinear correlations as well. In the mutual information function method τ is the first minimum of the function [17]

$$I(\tau) = - \sum_{h=1}^N \sum_{k=1}^N P_{h,k}(\tau) \ln \frac{P_{h,k}(\tau)}{P_h P_k}, \quad (12)$$

where P_h and P_k represent the probabilities that the variables assumes a value inside the h th and k th bins, respectively. $P_{h,k}(\tau)$ denote the joint probability that x_i is in bin h and $x_{i+\tau}$ is in bin k .

To obtain an estimate for the proper embedding dimension m , the method of false nearest neighbor (FNN) can be used [20]. In this method, for each point i in the time series, look for its nearest neighbor in the m dimensional space and compute the ratio of the distances between these points in m and $m + 1$ dimension as

$$\rho_{i,m} = \frac{|U(i) - U(j)|_{m+1}}{|U(i) - U(j)|_m}, \quad (13)$$

where $U(i), U(j)$ denote the state vectors at points i and j , and Euclidean norm is used. If this ratio is larger than a given threshold, then U_i is marked as having a false neighbor. The proper embedding dimension m is the value where FNN is close to zero.

4 Recurrence plots

The recurrence plots introduced by [14] is a graphical tool used for analyzing the dynamical properties of a time series obtained either from numerical simulation or experimental test rig. A recurrence plot (RP) is obtained from the recurrence matrix R whose entries can be given as

$$R_{ij} = \theta(\epsilon - \|y_i - y_j\|), \quad i, j = 1, \dots, N, \quad (14)$$

where $\|\cdot\|$ denote the distance between the two state vectors, ϵ is the predefined threshold value and θ is the Heaviside function. Depending on the value of the entries of R , either a black dot is drawn or a blank space is left in the RP. For computing the distance $\|\cdot\|$, different norms can be used (2-norm, max- norm). Dynamical features of the time series data can be extracted from the RPs [8, 25, 26]. For example, a periodic signal with mono-frequency are represented as equally spaced parallel lines (parallel to the main diagonal line) in RP. The RP of white noise is a homogeneous RP with no structure. Abrupt changes in the dynamics, laminarity of the time series and short term dynamics can be obtained from RPs [23, 25, 40]. The deterministic patterns of RPs based on the statics of the vertical and diagonal lines can be quantified using numbers with the method of Recurrence Quantification Analysis (RQA). The dynamics of the system can be identified using RQA method. In order to quantify the complexity of the RPs, we will use the following RQA parameters [23, 40]:

Reccurence rate (RR):

$$RR = \frac{1}{N^2} \sum_{i,j=1}^N R_{i,j}; \tag{15}$$

Determinism (DET):

$$DET = \frac{\sum_{l=l_{\min}}^N lP(l)}{\sum_{i,j=1}^N R_{i,j}}; \tag{16}$$

Entropy (ENT):

$$ENT = - \sum_{l=l_{\min}}^N p(l) \ln(p(l)); \tag{17}$$

Laminarity (LAM):

$$LAM = \frac{\sum_{v=v_{\min}}^N vP(v)}{\sum_{v=1}^N vP(v)}; \tag{18}$$

Averaged diagonal line length (L)

$$L = \frac{\sum_{l=l_{\min}}^N lP(l)}{\sum_{l=l_{\min}}^N P(l)}; \tag{19}$$

Trapping time (TT)

$$TT = \frac{\sum_{v=v_{\min}}^N vP(v)}{\sum_{v=v_{\min}}^N P(v)}. \tag{20}$$

$P(l)$, $P(v)$ represent the distribution of the lengths of diagonal lines and vertical lines, respectively. l_{\min} , v_{\min} denote e the minimum values of the diagonal and vertical line lengths, respectively. RR denotes the fraction of recurrence points in RPs. DET represents the fraction of recurrence points that form the diagonal lines. It gives a measure for predictability of the time series data. ENT is the Shannon entropy based the distribution of the lengths of diagonal lines. It captures the complexity of diagonal lines in RPs. For

higher values of ENT , the deterministic structure is more complex. LAM is the fraction of the points which form the vertical lines and represents the occurrence of laminar states in the system. TT is the trapping time which shows the average length of vertical lines. This gives an estimate for the mean time that the system will be trapped at a specific state.

5 Results and discussion

In the current study of pulsating magnetohydrodynamic mixed convection flow over a backward facing step, numerical simulation is performed for the range of parameters $25 \leq Re \leq 100$, $0 \leq Ha \leq 60$ and $0 \leq St \leq 1$. Grashof number is kept at constant value of $Gr = 10^4$. Amplitude of the forcing at the inlet is set to 0.75.

5.1 CFD results

Length averaged Nusselt number along the bottom wall downstream of the step plots are shown in Fig. 3 at Strouhal number of 0.1 for $Re = 25$ (top) and $Re = 100$ (bottom). The Nu values corresponding to different Ha numbers ($Ha = 0$, $Ha = 20$, $Ha = 60$) are plotted on each other. The time evolutions of the Nusselt numbers show that heat transfer is augmented and system reaches periodic steady state after certain time. Heat transfer enhancement is less effective as the Hartmann number increases. This could be attributed to the fact that flow velocity decreases as the Hartman number increases since magnetic field retards the convection. The time for the systems to reach periodic states (from initial transients) will increase when increasing the Reynolds number (Fig. 2 (bottom)). The convective time scale will decrease with increase in Reynolds number and the period of oscillation will increase with the increase in Reynolds number for the same Strouhal number. Another observation is that as Hartmann number increases, nonlinear distortions from a pure sinusoids will be suppressed more.

Figure 4 shows the time evolution of the averaged-Nusselt number along the bottom wall for Strouhal number of 1. The same trends as for $St = 0.1$ (Fig. 3) is also seen for different Ha numbers and Re numbers. When compared to the case at $St = 0.1$ for $Re = 25$ (Fig. 3 – top), the responses contain more harmonic contents at the same Ha numbers and for $Re = 100$ (Fig. 4 – bottom), the response is much weaker compared to cases for $Ha = 0$, $Ha = 20$.

Figure 5 shows several time instances within a period for the oscillation of the averaged Nusselt number at $Re = 100$, $Ha = 0$ and $St = 0.5$. The streamline plots for the time instances in Fig. 5 are depicted in Fig. 6. During the acceleration phase (Figs. 6a–6c), the core of the primary recirculation zone formed behind the step moves towards the step. At the point when the peak in the Nusselt number is achieved, the cell behind the step diminishes in size and gets more distorted from the upper part. Then the structure of the streamline patterns changes periodically. The isotherm plots for the same flow conditions and at the time instances according to Fig. 6 are shown in Fig. 7. The steepest temperature gradients are seen around the flow reattachment points. There is considerable change for shape of the isotherms in the vicinity of step. The level and direction of distortions of the isotherms change from point to point (points of Fig. 5).

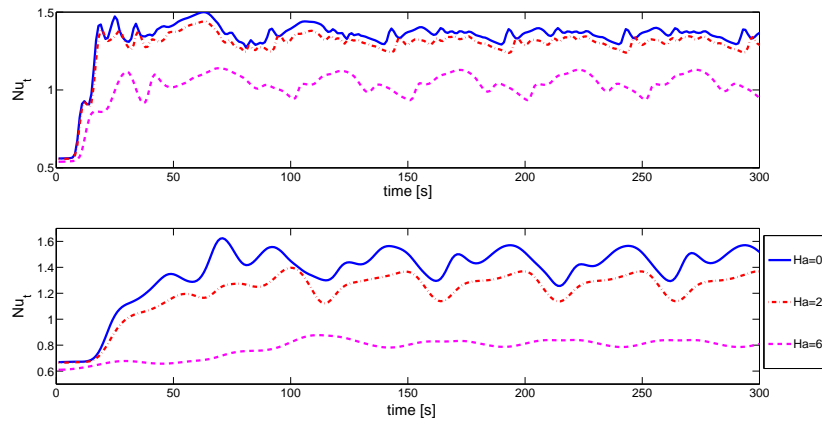


Fig. 3. Time evolution of the length averaged Nusselt number along the bottom wall downstream of the step for different Hartmann numbers at Strouhal number of 0.1 and at $Re = 25$ (top) and at $Re = 100$ (bottom).

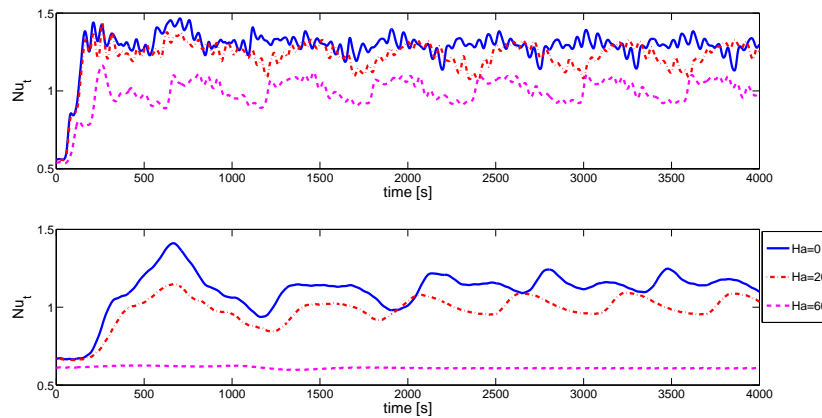


Fig. 4. Time evolution of the length averaged Nusselt number along the bottom wall downstream of the step for different Hartmann numbers at Strouhal number of 1 and at $Re = 25$ (top) and at $Re = 100$ (bottom).

Time-spatial averaged Nusselt number along the bottom wall downstream of the step (normalized with steady state values) versus Hartmann number plots are shown in Fig. 8 for various different Strouhal numbers at $Re = 25$ (top) and at $Re = 100$ (bottom). As the Hartmann number increases, heat transfer enhancement (HTE) decreases. The damping of the fluid motion and decrease in Nusselt number with increasing magnetic parameter is also supported with the studies given in [29]. HTE is more effective at Strouhal number of 0.1. This may be due to the adaptation of the system to its new flow condition with increasing frequency which decreases the heat transfer response of the system. The resonant type behavior of the heat transfer rate versus Strouhal number

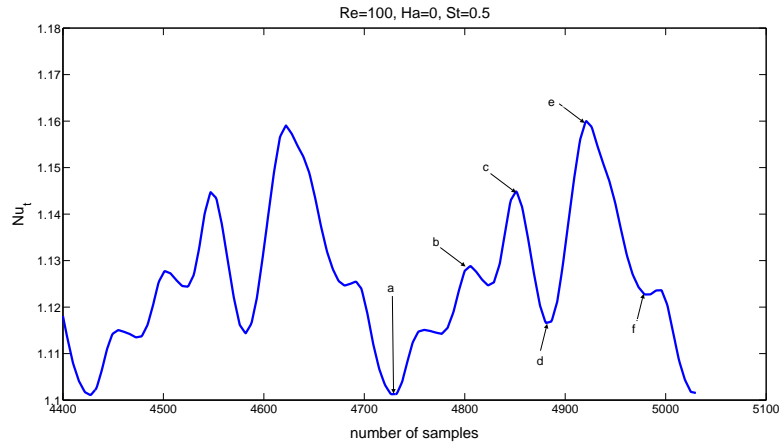


Fig. 5. Time instances within a period when the system reaches periodic steady state oscillation for parameter set ($Re = 100$, $Ha = 0$, $St = 0.5$).

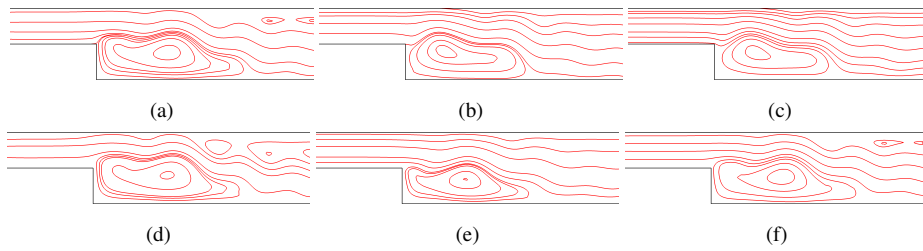


Fig. 6. Streamlines at the time instances according to Fig. 4 at ($Re = 100$, $Ha = 0$, $St = 0.5$).

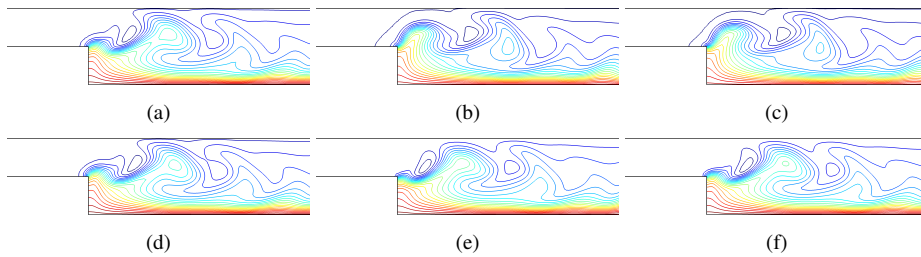


Fig. 7. Isotherms at the time instances according to Fig. 4 at ($Re = 100$, $Ha = 0$, $St = 0.5$).

for pulsating flow of backward facing step is already observed in [31]. The heat transfer behavior for the considered range of range of St number in this study, (between 0.1 and 1) is supported with the results given in [31]. The maximum and minimum HTE are 242 percent and -1 percent at the set of parameters ($Re = 25$, $Ha = 0$ and $St = 0.1$) and ($Re = 100$, $Ha = 60$ and $St = 1$).

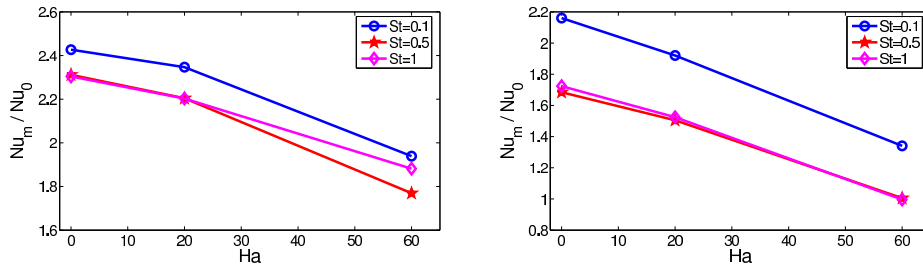


Fig. 8. Variation of the normalized averaged Nusselt number along the bottom wall for different Strouhal numbers at $Re = 25$ (top) and $Re = 100$ (bottom).

5.2 Nonlinear time series results

In this part, dynamical analysis of the MHD pulsating flow in backward facing step geometry is conducted. The FFT plots for the nonlinear time series data of the averaged Nusselt numbers when the initial transients are removed (when the system reaches periodic steady states) are shown for different Ha and Re numbers in Fig. 9 for Strouhal number of 0.1 and in Fig. 10 for Strouhal number of 1. In Fig. 9, at the parameter set ($Re = 25$, $Ha = 0$, $St = 0.1$), there exists higher harmonic contents in the periodic signal which are at the integer multiples of forcing frequency (Fig. 9a). As the Hartmann number increases, nonlinearity decreases and the amplitude of the higher harmonics decreases (Fig. 9b). At the parameter set ($Re = 100$, $Ha = 0$, $St = 0.1$), there exist a peak which is not the integer multiple of fundamental harmonic. The results in Fig. 10 shows that only at the parameter set ($Re = 100$, $Ha = 60$, $St = 1$), the fundamental harmonic appears

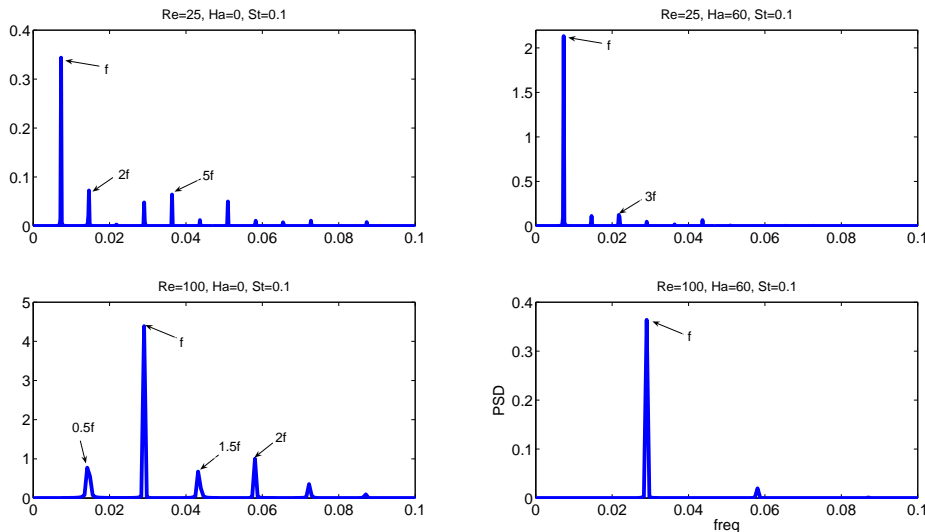


Fig. 9. Frequency spectrum of the time series data (averaged Nusselt number along the bottom wall) for different Reynolds and Hartmann numbers at Strouhal number of 0.1.

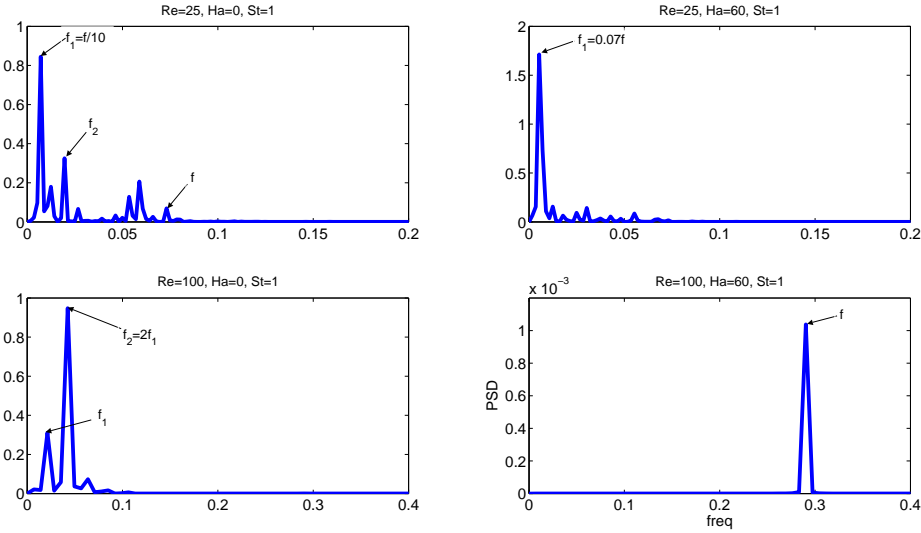


Fig. 10. Frequency spectrum of the time series data (averaged Nusselt number along the bottom wall) for different Reynolds and Hartmann numbers at Strouhal number of 1.

Table 3. Optimal embedding dimensions (m) and embedding delays (τ) for different combination of parameters.

| Parameters | | | Embedding delay | Embedding dimension |
|------------|------|------|-----------------|---------------------|
| Re | Ha | St | | |
| 25 | 0 | 0.1 | 1 | 3 |
| 25 | 60 | 0.1 | 2 | 3 |
| 100 | 0 | 0.1 | 2 | 3 |
| 100 | 60 | 0.1 | 3 | 3 |
| 25 | 0 | 1 | 6 | 6 |
| 25 | 60 | 1 | 10 | 5 |
| 100 | 0 | 1 | 22 | 5 |
| 100 | 60 | 1 | 3 | 3 |

whereas for the other combination of parameters at $St = 1$, incommensurate frequencies are seen and the fundamental frequency disappears. These results show the complicated interaction of the magnetic field and pulsating flow for a backward facing step geometry.

The proper embedding dimension m and embedding delay τ parameters are calculated as described in the previous sections for each of the parameter sets and are tabulated in Table 3. Fig. 11 depicts the mutual information function for parameter sets ($Re = 25$, $Ha = 0$, $St = 0.1$) and ($Re = 25$, $Ha = 60$, $St = 0.1$) with respect to delay parameter and as can be seen the first minimum of the functions are seen at $\tau = 2$ and $\tau = 3$. The percentage of false neighbors (fnn) calculated for increasing reconstruction dimensions are shown in Fig. 12 for parameter sets ($Re = 25$, $Ha = 0$, $St = 0.1$) and ($Re = 25$, $Ha = 60$, $St = 0.1$). These plots show for embedding dimension of 3, these percentages go very close to zero. These plots show that the dynamics of oscillations in is restricted to a three-dimensional phase space.

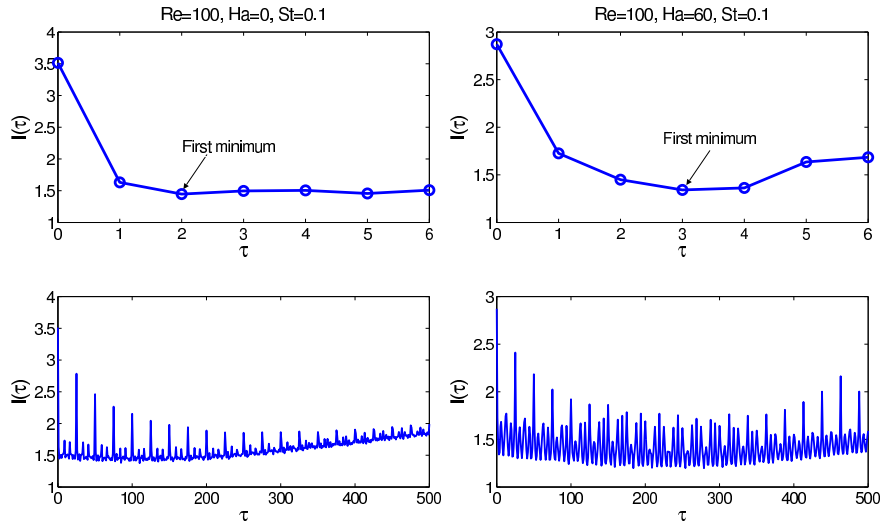


Fig. 11. Proper embedding delay determination for left – ($Re = 100, Ha = 0, St = 0.1$) and right – ($Re = 100, Ha = 60, St = 0.1$). The first minimum of the mutual informations are seen at $\tau = 2$ and $\tau = 3$.

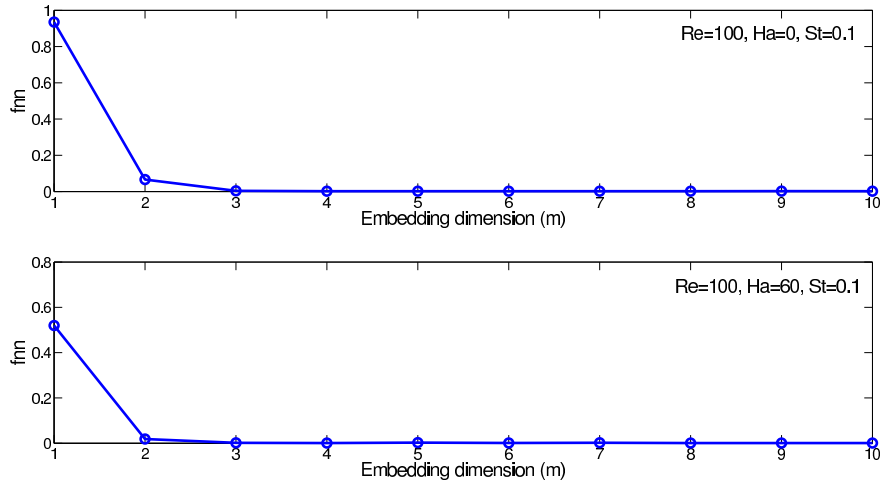


Fig. 12. Minimal required embedding dimension determination for top – ($Re = 100, Ha = 0, St = 0.1$) and bottom – ($Re = 100, Ha = 60, St = 0.1$). False nearest neighbors (fnn) drop to zero at $m = 3$.

Figures 13 and 14 show the RPs of the nonlinear time series for the averaged Nusselt number along the bottom wall for different Hartmann numbers and Strouhal numbers at $Re = 25$ and $Re = 100$, respectively. The RPs and RQA are carried out using the software developed by [24]. In the RPs, equally spaced diagonal lines represent the presence of a single frequency in the oscillation. In Figs. 13a, b, a series of lines with parallel to the main diagonal which indicate a more regular oscillatory behavior is seen.

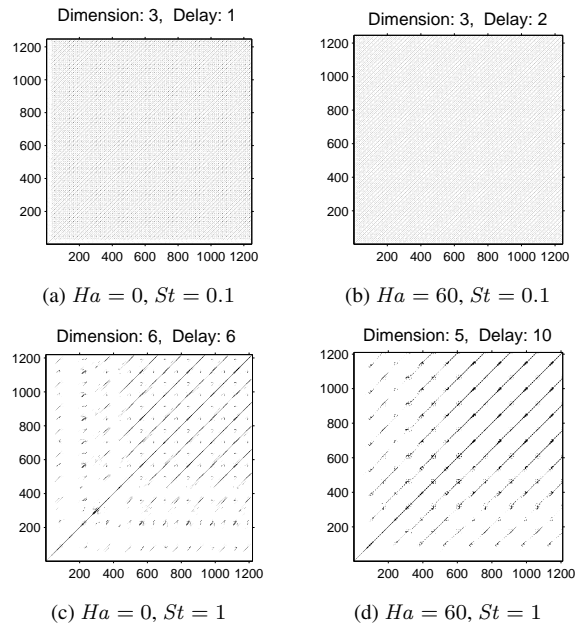


Fig. 13. Recurrence plots of the averaged Nusselt number time series at $Re = 25$ for different Hartmann and Strouhal numbers.

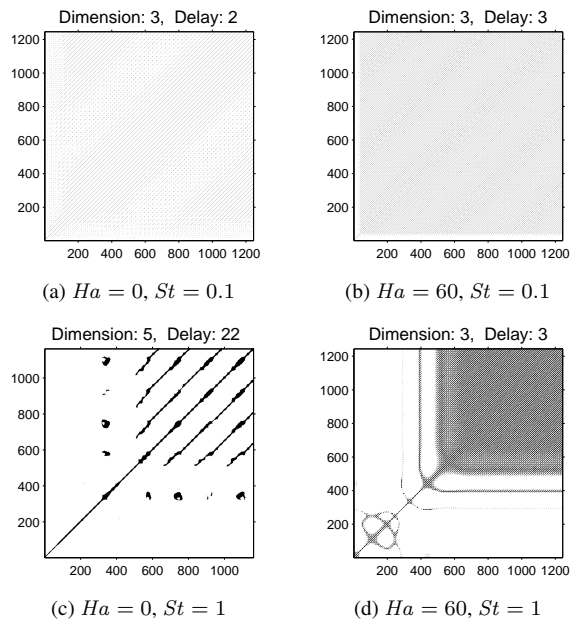


Fig. 14. Recurrence plots of the averaged Nusselt number time series at $Re = 100$ for different Hartmann and Strouhal numbers.

Table 4. RQA parameter values for different combinations of Re , Ha and St numbers.

| Parameters | | | RR | DET | L | ENT | LAM | TT |
|------------|------|------|--------|-------|-------|-------|-------|------|
| Re | Ha | St | | | | | | |
| 25 | 0 | 0.1 | 0.0467 | 0.827 | 5.59 | 1.69 | 0.25 | 2.58 |
| 25 | 60 | 0.1 | 0.0445 | 0.684 | 14.59 | 2.25 | 0.09 | 2.01 |
| 100 | 0 | 0.1 | 0.0251 | 0.846 | 12.35 | 2.37 | 0.008 | 2.01 |
| 100 | 60 | 0.1 | 0.0679 | 0.978 | 16.81 | 1.64 | 0.082 | 2.03 |
| 25 | 0 | 1 | 0.0067 | 0.921 | 7.01 | 1.94 | 0.764 | 2.78 |
| 25 | 60 | 1 | 0.0114 | 0.961 | 7.67 | 2.23 | 0.88 | 3.34 |
| 100 | 0 | 1 | 0.0227 | 0.998 | 26.91 | 3.47 | 0.99 | 7.58 |
| 100 | 60 | 1 | 0.126 | 0.961 | 14.71 | 2.15 | 0.99 | 4.04 |

The presence of a second frequency which is not at integer multiple of the fundamental frequency translates the diagonal lines parallel to main diagonal but separated by unequal vertical spacing. The structures in Figs. 13c, d shows a content of high frequency oscillations. In Fig. 14b, the presence of a dominant frequency is seen with the lines parallel to the main diagonal. In Fig. 14a, the separation of diagonally orientated lines by unequal vertical spacing indicates the presence of a second frequency. The RP structure for Strouhal number of 1 at $Re = 100$ (Figs. 14c, d) is different compared to other RPs. In Fig. 14c, the paling of the plot away from the diagonal during 400 time samples indicate the non-stationarity of the data set and then diagonally oriented lines indicate the periodicity of the data set.

Table 4 shows the QRA analysis results for different combinations of parameters. A higher ENT value indicates higher structural complexity and its value increases with increasing Reynolds number and Strouhal numbers. ENT attains its largest value at parameter set ($Re = 100$, $Ha = 0$, $St = 1$). The smallest value of TT indicates the shortest time in the laminar phase in the intermittent dynamics which is obtained at Strouhal number of 0.1. The largest values of LAM are obtained for Strouhal number of 1. The higher values of DET represents the higher predictability of the system. These results show that dynamical behavior of the complex system with MHD and pulsating flow over a backward facing step can be identified by using RQA method.

6 Conclusions

In this study, pulsating magnetohydrodynamic mixed convection over a backward facing step is numerically investigated for a range of Reynolds, Hartmann and Strouhal numbers and recurrence quantification analysis is employed for the time series data of the averaged-Nusselt number along the bottom wall of the cavity. The obtained results can be summarized as:

- As the Hartmann number increases, heat transfer enhancement (HTE) decreases.
- As the pulsating frequency increases, HTE decreases due to the adaptation of the system to its new flow condition with increasing frequency.
- At the parameter set ($Re = 100$, $Ha = 60$, $St = 1$), the fundamental forcing frequency appears whereas for the other combination of parameters at $St = 1$,

incommensurate frequencies are seen and the fundamental frequency disappears.

- As the Hartmann number increases, nonlinearity (for the input (pulsating velocity at the inlet)-output (averaged Nusselt number along the bottom wall downstream of the step) relation) decreases and the amplitude of the higher harmonics decreases.
- Pulsating flow and magnetic field parameters can be utilized to control the heat transfer and fluid flow for the backward facing step configuration.
- The recurrence plots for time series data of averaged Nusselt number shows different structures in the plots indicating different dynamic features of the systems.
- The recurrence quantification analysis for the time series of Nusselt number reveals different parameters quantifying structural complexity, predictability and time in the laminar phase in the intermittent dynamic for different combinations of parameters.

References

1. H. Abu-Mulaweh, A review of research on laminar mixed convection flow over backward- and forward facing steps, *Int. J. Therm. Sci.*, **42**:897–909, 2003.
2. H. Abu-Mulaweh, Turbulent mixed convection flow over a forward-facing step –the effect of step heights, *Int. J. Therm. Sci.*, **44**:155–162, 2005.
3. S. Acharya, G. Dixit, Q. Hou, Laminar mixed convection in a vertical channel with a backstep: A benchmark study, in B.F. Blackwell, B.F. Armaly (Eds.), *Computational Aspects of Heat Transfer Benchmark Problems: Presented at the 1993 ASME Winter Annual Meeting, New Orleans, Louisiana, November 28–December 3, 1993*, ASME HTD Vol. 258, ASME, New York, 1993, pp. 11–20.
4. B.F. Armaly, F. Durst, J.C.F. Pereira, B. Schonung, Experimental and theoretical investigation of backward-facing step flow, *J. Fluid Mech.*, **127**:473–496, 1983.
5. O. Aydin, A. Kaya, MHD-mixed convection from a vertical slender cylinder, *Commun. Nonlinear Sci. Numer. Simul.*, **16**(4):1863–1873, 2011.
6. J.G. Barbosa-Saldana, N.K. Anand, Flow over a three-dimensional horizontal forward-facing step, *Numer. Heat Transfer, Part A*, **53**:1–17, 2008.
7. D. Barkley, M. Gabriela, M. Gomes, R.D. Henderson, Three-dimensional instability in flow over a backward-facing step, *J. Fluid Mech.*, **473**:167–190, 2002.
8. M. Casdagli, Recurrence plots revisited, *Physica D*, **108**:12–44, 1997.
9. T.P. Chiang, T.W.H. Sheu, A numerical revisit of backward-facing step flow problem, *Phys. Fluids*, **11**:862–874, 1999.
10. R. Cochran, R. Horstman, Y. Sun, A. Emery, Benchmark solution for a vertical buoyancy-assisted laminar backward-facing step flow using finite element, finite volume and finite difference methods, in B.F. Blackwell, B.F. Armaly (Eds.), *Computational Aspects of Heat Transfer Benchmark Problems: Presented at the 1993 ASME Winter Annual Meeting, New Orleans, Louisiana, November 28–December 3, 1993*, ASME HTD Vol. 258, ASME, New York, 1993, pp. 37–47.

11. Comsol AB, COMSOL FEMLAB 3.2 User's Guide, 2005.
12. D. Das, J.H. Arakeri, Transition of unsteady velocity profiles with reverse flow, *J. Fluid Mech.*, **374**:251–283, 1998.
13. B. Dyne, D. Pepper, F. Brueckner, Mixed convection in a vertical channel with a backward-facing step, in B.F. Blackwell, B.F. Armaly (Eds.), *Computational Aspects of Heat Transfer Benchmark Problems: Presented at the 1993 ASME Winter Annual Meeting, New Orleans, Louisiana, November 28–December 3, 1993*, ASME HTD Vol. 258, ASME, New York, 1993, pp. 49–56.
14. J. Eckmann, S. Kamphorst, D. Ruelle, Recurrence plots of dynamical systems, *Europhys. Lett.*, **5**:973–977, 1987.
15. M. El-Refaee, M. El-Sayed, N. Al-Najem, I. Megahid, Steady-state solutions of buoyancy-assisted internal flows using a fast false implicit transient scheme (fits), *Int. J. Numer. Methods Heat Fluid Flow*, **6**:3–23, 1996.
16. E. Erturk, Numerical solutions of 2-d steady incompressible flow over a backward-facing step, Part I: High reynolds number solutions, *Comput. Fluids*, **37**:633–655, 2008.
17. A.M. Fraser, H. Swinney, Independent coordinates for strange attractors from mutual information, *Phys. Rev. A*, **33**:1134–40, 1986.
18. M. Hino, M. Sawamoto, S. Takasu, Experiments on transition to turbulence in an oscillatory pipe flow, *J. Fluid Mech.*, **75**:193–207, 1976.
19. A. Ishak, R. Nazar, I. Pop, Mhd convective flow adjacent to a vertical surface with prescribed wall heat flux, *Int. Commun. Heat Mass Transfer*, **36**:554–557, 2009.
20. M. Kennel, R.B.H. Abarbanel, Determining embedding dimension for phase space reconstruction using a geometrical construction, *Phys. Rev. A*, **45**:3403–11, 1992.
21. A. Kumar, A.K. Dhiman, Effect of a circular cylinder on separated forced convection at a backward-facing step, *Int. J. Therm. Sci.*, **52**:176–185, 2012.
22. J. Lin, B. Armaly, T. Chen, Mixed convection in buoyancy-assisted vertical backward-facing step flows, *Int. J. Heat Mass Transfer*, **33**:2121–2132, 1990.
23. N. Marwan, *Encounters with Neighbors: Current Developments of Concepts Based on Recurrence Plots and Their Applications*, PhD thesis, University of Potsdam, 2003.
24. N. Marwan, Recurrence plots code, <http://www.agnld.uni-potsdam.de/marwan/6.download/rp.phpS>, 2006.
25. N. Marwan, A. Meinke, Extended recurrence plot analysis and its application to erp data, *Int. J. Bifurcation Chaos Appl. Sci. Eng.*, **14**:761–771, 2004.
26. N. Marwan, N. Wessel, U. Meyerfeldt, A. Schirdewan, J. Kurths, Recurrence plot-based complexity and their application to heartrate variability data, *Phys. Rev. E*, **66**, 026702, 2002.
27. H.F. Oztop, K.A.-S.I. Pop, Mhd mixed convection in a lid-driven cavity with corner heater, *Int. J. Heat Mass Transfer*, **54**:494–3504, 2011.
28. M. Pirmohammadi, M. Ghassemi, Effect of magnetic field on convection heat transfer inside a tilted square enclosure, *Int. Commun. Heat Mass Transfer*, **36**:776–780, 2009.

29. M. Rahman, H.F. Oztop, R. Saidur, S. Mekhilef, K. Al-Salem, Finite element solution of mhd mixed convection in a channel with a fully or partially heated cavity, *Comput. Fluids*, **79**:53–64, 2013.
30. F. Selimefendigil, H.F. Oztop, Identification of forced convection in pulsating flow at a backward facing step with a stationary cylinder subjected to nanofluid, *Int. Commun. Heat Mass Transfer*, **45**:111–121, 2013.
31. F. Selimefendigil, H.F. Oztop, Numerical analysis of laminar pulsating flow at a backward facing step with an upper wall mounted adiabatic thin fin, *Comput. Fluids*, **88**:93–107, 2013.
32. F. Selimefendigil, H.F. Oztop, Control of laminar pulsating flow and heat transfer in backward facing step by using a square obstacle, *J. Heat Transfer*, **136**, 081701, 2014.
33. F. Selimefendigil, H.F. Oztop, Effect of a rotating cylinder in forced convection of ferrofluid over a backward facing step, *Int. J. Heat Mass Transfer*, **71**:142–148, 2014.
34. F. Selimefendigil, H.F. Oztop, Mhd mixed convection of nanofluid filled partially heated triangular enclosure with a rotating adiabatic cylinder, *J. Taiwan Inst. Chem. Eng.*, **45**:2150–2162, 2014.
35. F. Selimefendigil, H.F. Oztop, Numerical study of mhd mixed convection in a nanofluid filled lid driven square enclosure with a rotating cylinder, *Int. J. Heat Mass Transfer*, **78**:741–754, 2014.
36. F. Selimefendigil, H.F. Oztop, K. Al-Salem, Natural convection of ferrofluids in partially heated square enclosures, *J. Magn. Magn. Mater.*, **372**:122–133, 2014.
37. M. Sherry, D. LoJacono, J. Sheridan, An experimental investigation of the recirculation zone formed downstream of a forward facing step, *J. Wind Eng. Ind. Aerodyn.*, **98**:888–894, 2010.
38. F. Takens, *Detecting strange attractors in turbulence*, in *Dynamical Systems and Turbulence, Warwick 1980*, Lect. Notes Math., Vol. 898, Springer, Berlin, 1981, pp. 366–381.
39. S. Terhaar, A. Velazquez, J. Arias, M. Sanchez-Sanz, Experimental study on the unsteady laminar heat transfer downstream of a backwards facing step, *Int. Commun. Heat Mass Transfer*, **37**:457–462, 2010.
40. C. Webber, J. Zbilut, Dynamical assessment of physiological systems and states using recurrence plot strategies, *J. Appl. Physiol.*, **76**:965–973, 1994.
41. P. Williams, A.J. Baker, Numerical simulations of laminar flow over a 3d backward-facing step, *Int. J. Numer. Methods Fluids*, **24**:1159–1183, 1997.